Pergamon

Int. J. Solids Structures Vol. 35, No 30, pp. 3989–4000, 1998

0020–7683/98 $19.00 + .00

PII: S0020–7683(97)00254–0

INTERACTION OF VERY SMALL VOIDS WITH LARGER VOIDS

VIGGO TVERGAARD
Department of Solid Mechanics, Technical University of Denmark, DK-2800 Lyngby, Denmark

(*Received* 17 *April* 1997; *in revised form* 14 *August* 1997)

Abstract—For a very small void in the material between much larger voids the influence of local stress increases induced by the larger voids is studied numerically. The point of interest is whether or not such local stress increases result in a cavitation instability at the tiny void, even if the average overall stress levels are well below those required for unstable cavity growth. The analyses are based on an axisymmetric unit cell model with special boundary conditions, which allow for a relatively simple investigation of a full three dimensional array of spherical voids, without having to solve the full 3D numerical problem. For overall stress levels as large as those reached ahead of a blunting crack tip, a cavitation instability at the small void, induced by interaction with the large voids, is not found here. But the results show that localization of plastic flow in the unit cell plays an important role. © 1998 Elsevier Science Ltd. All rights reserved.

1. INTRODUCTION

In studies of ductile fracture mechanisms for metals the analysis of void growth to coalescence plays an important role. Early investigations considered the growth of a single void in an infinite elastic-plastic solid (McClintock, 1968; Rice and Tracey, 1969), whereas later micromechanical studies have incorporated the interaction between neighbouring voids and the effect of a finite volume fraction of voids, by analysing a cell model representative of a material containing a periodic array of identical voids (Needleman, 1972; Tvergaard, 1981, 1982a; Koplik and Needleman, 1988). Some of the analyses have been carried out for cylindrical voids under transverse loading, while other studies consider more realistic shapes, such as initially spherical voids.

In real void containing materials there is a distribution of void sizes, resulting from different sizes of the inclusions at which the voids nucleate, different amounts of growth since nucleation of each void, etc. To gain some insight in the effect of different void sizes, Tvergaard (1996a) has recently used a special axisymmetric cell model to study a material, where a large void is surrounded by smaller voids, and vice versa. This cell model is analogous to a model introduced to study metal matrix composites with a transversely staggered array of reinforcing short fibres (Tvergaard, 1990). Various void size differences were considered, with the larger void volume up to seven times that of the smaller void, and it was found that interaction can lead to significant differences between the growth rates of different size voids, except in a range of very small void volume fractions where interaction disappears. At very high stress triaxialities, where a cavitation instability is expected (Ball, 1982; Ashby *et al.*, 1989; Huang *et al.*, 1991; Tvergaard *et al.*, 1992), it was found that only one of the voids in the unit cell grows very large in an unstable manner, while the other void stops growing.

Much larger initial void size differences have been considered by Faleskog and Shih (1997), who have used a plane strain model with parallel cylindrical voids. These authors have focused on the fact that the stress levels in the region between two larger voids are increased relative to the average stress state in the material, and therefore a very small void growing in this region can experience unstable growth, even when the average stress levels in the material are well below the cavitation instability level. This idea is interesting, as it could possibly explain occurrence of unstable cavity growth in front of a blunting crack tip in a homogeneous elastic–plastic material, even though the peak stress levels at a blunting

crack tip are well below the stress levels required for cavitation instabilities to occur. However, these predictions rely on the cylindrical void shape, which is not very realistic. If the void shapes are more like spherical, it is expected that the stress increase between two larger voids will decay much more rapidly with increasing void spacing.

In the present paper the axisymmetric cell model of Tvergaard (1996) is used to investigate the behaviour of very small voids growing in the region between two larger growing voids. This cell model is able to represent reasonably realistic spherical void shapes, and therefore the study allows for an evaluation of how the effect proposed by Faleskog and Shih (1997) would depend on deviations from their assumption of cylindrical voids. Although the cell models presume macroscopically uniform stress states, the results will be used here to draw some conclusions on the effect of different void sizes interacting in a blunting crack tip region.

2. PROBLEM FORMULATION AND NUMERICAL METHOD

The axisymmetric cell model to be used here is identical to that used in Tvergaard (1996), considering a periodic array of voids as illustrated in Fig. 1. The voids of two different sizes are initially spherical with radii R_1 and R_2, they have the spacing A_0 in the axial direction and the spacings B_0 in the two transverse directions. The main difference from the previous computation is that in the present paper the small voids are much smaller than the larger ones, and that the spacing A_0 in axial direction is taken to be significantly larger than the spacing B_0 in transverse direction. Thus, the cell model is here used to analyse a material with layers of voids normal to the axial direction, where the layers are so well separated from one another that there is practically no interaction between them. The focus here is on interaction between different size voids in one of the layers, which could represent voids in the plane of a growing crack, ahead of the crack tip.

The use of the axisymmetric unit cell to analyse materials with transversely staggered fibres or voids has been discussed in detail by Tvergaard (1990, 1996), and therefore only a few basic relations will be reviewed here. The initial radius of the axisymmetric unit cell is chosen as $R_0 = B_0/\pi^{1/2}$, in order that the void volume fraction of the cell is equal to that of the model material in Fig. 1. The cell model (Fig. 2) is analysed in a cylindrical reference

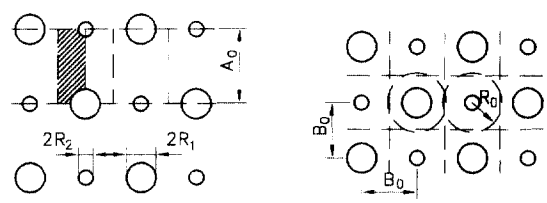

Fig. 1. Periodic array of spherical voids with two different void sizes. (a) Cross-section along axial direction, with void spacing A_0. (b) Cross section normal to axial direction, with cell radius R_0. Most computations here are carried out for $A_0/R_0 = 10$.

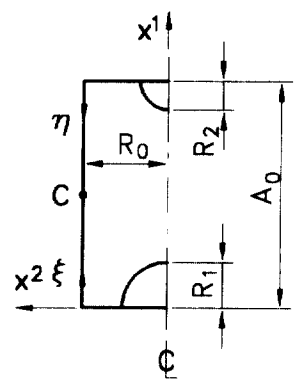

Fig. 2. Axisymmetric cell model analysed numerically, with x^1 along the axial direction.

coordinate system, where x^1 and x^2 are the axial and radial coordinates, while x^3 is the circumferential angle. The displacement components and the nominal traction components on reference base vectors are denoted by u^i and T^i. The symmetry boundary conditions at the ends of the cell are

$$u^1 = -\frac{U}{2}, \quad T^2 = 0 \text{ at } x^1 = 0 \tag{2.1}$$

$$u^1 = -\frac{U}{2}, \quad T^2 = 0 \text{ at } x^1 = A_0 \tag{2.2}$$

where U is a constant. As the neighbouring cell is identical to the cell analysed but is rotated 180° so that its x^1 axis points in the opposite direction (see Fig. 1a), compatibility in the axial direction requires that

$$u^1(\xi) = -u^1(\eta), \quad \text{for } \xi = \eta, \quad x^2 = R_0 \tag{2.3}$$

Here, ξ and η are distances from the bottom and the top, respectively, of the cell in the reference state (Fig. 2). Radial compatibility requires that the total cross-sectional area is independent of the x^1 coordinate

$$[R_0 + u^2(\xi)]^2 + [R^0 + u^2(\eta)]^2 = 2(R_0 + u_C^2)^2, \quad \text{for } \xi = \eta, \quad x^2 = R_0 \tag{2.4}$$

where u_C^2 is the radial displacement at the centre point C indicated in Fig. 2. The equilibrium conditions on the cell side are specified as

$$T^1(\xi) = T^1(\eta), \quad T^2(\xi) = T^2(\eta), \quad \text{for } \xi = \eta, \quad x^2 = R_0 \tag{2.5}$$

The average logarithmic strains in the axial and transverse directions are $\varepsilon_1 = \ln(1 + U/l_c)$ and $\varepsilon_2 = ln(1 + u_C^2/R_0)$, respectively.

The average nominal stresses Σ_{ij} are computed as the appropriate area averages of the microscopic nominal stress components on the surface, noting that it is necessary to average over both the cell analysed and one of the neighbouring cells of opposite kind. The axial and transverse Cartesian stress components are Σ_{11} and $\Sigma_{22} = \Sigma_{33}$, respectively, for the axisymmetric problem and all shear components vanish. Using the average strains ε_1 and ε_2, the average true stresses σ_1 and σ_2 are calculated from the nominal stress values.

When A_0 is much larger than B_0, so that there is no void interaction in the axial direction, it may appear that the model could be further simplified by cutting in the middle of the unit cell and analysing on each side of the cut individually. However, the interaction of two neighbouring cylindrical cell models with different size voids would still have to be accounted for, which would require boundary conditions like eqns (2.3)–(2.5). Therefore, such an alternative strategy would not really represent a simplification.

The volume fractions of voids have been used by Tvergaard (1996) to specify void growth behaviour, but these values are less relevant when the cell model is used to describe interactions inside an isolated layer of voids. If the layer thickness is taken to be $2R_0$, the initial volume fractions inside the layer $(f_1^*)_I$ and $(f_2^*)_I$ for the larger and smaller voids, respectively, are

$$(f_1^*)_I = \frac{R_1^3}{3R_0^3}, \quad (f_2^*)_I = \frac{R_2^3}{3R_0^3} \tag{2.6}$$

and the total initial void volume fraction inside the layer is $f_I^* = (f_1^*)_I + (f_2^*)_I$. It is noted that multiplication of the values in (2.6) by $2R_0/A_0$ gives the actual initial void volume

fractions in the model material. In the present paper it will be more practical to specify void growth in terms of the relative void volumes v_1 and v_2 defined by

$$v_1 = (V/V_I)_1, \quad v_2 = (V/V_I)_2 \tag{2.7}$$

where V_I and V denote the initial and current void volumes, respectively. The initially larger void is denoted void No. 1.

It is noted that the use of a unit cell model enforces periodicity of the solution throughout the deformation history. Thus, plastic flow localization can be represented, if the periodicities are satisfied, but more general localization modes are excluded by the procedure employed here.

The material is described by J_2 flow theory with isotropic hardening. A convected-coordinate lagrangian formulation of the field equations is used, in which g_{ij} and G_{ij} are metric tensors in the reference configuration and the current configuration, respectively, with determinants g and G, and $\eta_{ij} = \frac{1}{2}(G_{ij} - g_{ij})$ is the lagrangian strain tensor. The contravariant components τ^{ij} of the Kirchhoff stress tensor on the current base vectors are related to the components of the Cauchy stress tensor σ^{ij} by $\tau^{ij} = (G/g)^{1/2}\sigma^{ij}$. Then, in the finite strain generalization of J_2 flow theory the incremental stress–strain relationship is of the form $\dot{\tau}^{ij} = L^{ijkl}\dot{\eta}_{kl}$, where the tensor of instantaneous moduli can be found in Hutchinson (1973) or Tvergaard (1996). The uniaxial stress–strain behaviour is represented by

$$\varepsilon = \begin{cases} \dfrac{\sigma}{E} & \text{for } \sigma \leqslant \sigma_y \\ \dfrac{\sigma_y}{E}\left(\dfrac{\sigma}{\sigma_y}\right)^{1/N} & \text{for } \sigma > \sigma_y \end{cases} \tag{2.8}$$

where σ_y is the uniaxial yield stress, E is Young's modulus and N is the strain-hardening exponent. The tangent modulus E_t is the slope of the true stress vs. natural strain curve at the stress level σ_e.

Equilibrium is specified in terms of the principle of virtual work

$$\int_V \tau^{ij}\delta\eta_{ij}\,\mathrm{d}V = \int_S T^i\delta u_i\,\mathrm{d}S \tag{2.9}$$

where V and S denote the reference volume and surface of the cell analysed, T^i are the specified nominal surface tractions, and u^i are the displacement components on the base vectors of the cylindrical reference coordinate system. In terms of the displacement components the lagrangian strain tensor is given by

$$\eta_{ij} = \frac{1}{2}(u_{i,j} + u_{j,i} + u^k_{,i}u_{k,j}) \tag{2.10}$$

where $(\,)_{,j}$ denotes the covariant derivative in the reference frame. Approximate solutions of (2.9) are obtained by a linear incremental method, using a finite element approximation of the displacement fields. The elements used are quadrilaterals each built up of four triangular axisymmetric linear-displacement elements. A fixed ratio ρ is enforced between the average true stress σ_2 and σ_1 in the transverse and axial directions respectively

$$\sigma_2 = \rho\sigma_1 \tag{2.11}$$

A special Rayleigh–Ritz finite element method (Tvergaard, 1976) is used to implement the boundary conditions, and also in some cases to prescribe a node displacement on one of the void surfaces rather than the end displacement U, without applying a load on the void

surface. This improves the numerical stability near the occurrence of a cavitation instability, where $\dot{U} \to 0$.

3. RESULTS

The materials to be analysed here are characterized by the material parameters $\sigma_y/E = 0.003$ and $N = 0.1$, and the value of Poisson's ratio is taken to be $\nu = 0.3$. The ratio of the average true stresses, $\rho = \sigma_2/\sigma_1$, is kept fixed in each case studied. Furthermore, the initial mesh for different size voids is chosen such that relative to void size the meshes around each void are nearly identical (see Fig. 3a). Thus, the number of elements and the element size stretching along the void surface are identical for the two voids, and also in radial direction the number of elements and the stretching are chosen to give equal size elements relative to the different void radii. It has been found that such closely identical meshes, relative to void size, are important in order to minimize the effect of mesh on the predicted differences between the rates of growth of different size voids (Tvergaard, 1996).

In the first cases to be discussed the initial volume of the larger void is 7.0 times that of the smaller void, so that $(f_1^*/f_2^*)_I = 7.0$, or $(f_1^*/f^*)_I = 0.875$. Furthermore, the void spacing in axial direction is taken to be ten times the radius of the unit cell, $A_0/R_0 = 10$. Thus, although the void spacings in the axial direction are relatively larger here, the void size ratios are the same as those studied in several analyses of Tvergaard (1996a), and therefore the interactions between neighbouring voids in the transverse direction should be comparable. The principal stress ratio is here taken to be $\rho = 0.5$, and the computations are illustrated in Figs 3 and 4.

Fig. 3 shows the initial undeformed mesh and three deformed meshes for a case where $f_I^* = 0.04$, which corresponds to $R_1/R_0 = 0.472$. Stress–strain curves and curves describing the void growth are shown in Fig. 4 for the same case, $f_I^* = 0.04$, together with similar

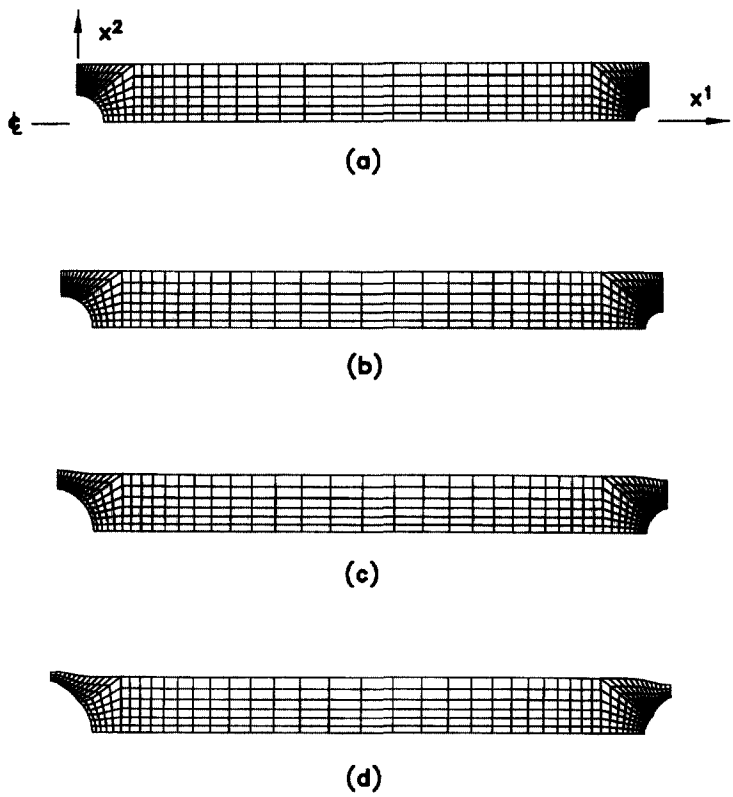

Fig. 3. Initial and deformed meshes for $A_0/R_0 = 10$, $\rho = 0.5$, $f_I^* = 0.04$ and $(f_1^*/f_2^*)_I = 7.0$. (a) At $\varepsilon_1 = 0$, $\sigma_1/\sigma_y = 0$. (b) At $\varepsilon_1 = 0.051$, $\sigma_1/\sigma_y = 2.45$. (c) At $\varepsilon_1 = 0.064$, $\sigma_1/\sigma_y = 1.97$. (d) At $\varepsilon_1 = 0.080$, $\sigma_1/\sigma_y = 1.14$.

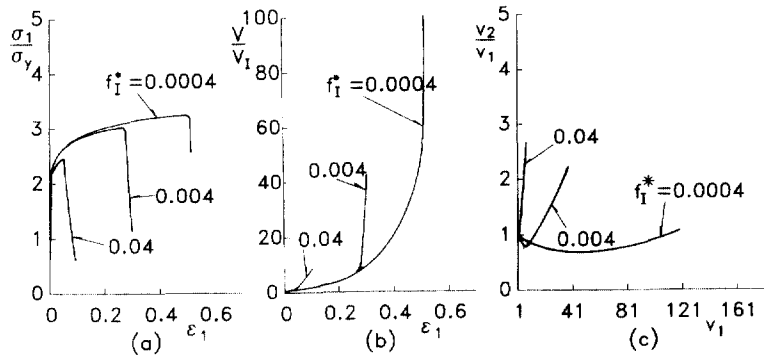

Fig. 4. Stress–strain curves and void growth for $A_0/R_0 = 10$, $\rho = 0.5$ and $(f_1^*/f_2^*)_I = 7.0$. (a) Axial tensile stress vs strain. (b) Total void volume vs strain. (c) Growth of normalized void volumes.

curves for 10 times smaller voids and for 100 times smaller voids, respectively. Here, V/V_1 denotes the sum of the void volumes divided by the initial sum, whereas v_1 and v_2 are similar ratios (2.7) for the larger void and the smaller void, respectively. Fig. 3b shows the deformed mesh at the maximum stress point, where $\varepsilon_1 = 0.051$, $\sigma_1/\sigma_y = 2.45$, $V/V_I = 1.633$, $v_1 = 1.626$, and $v_2/v_1 = 1.038$. Immediately after this point localization of plastic flow occurs in the layers containing the voids, so that most of the unit cell between the two voids experiences elastic unloading. Figs 4a and 4b show that this localization gives rapidly increasing void growth at the same time as the average tensile stress decays abruptly. Fig. 4c shows that after localization the smaller void starts to grow much more rapidly than the larger one, as can also be seen in Figs 3c and 3d. At the last stage, Fig. 3d, where $\varepsilon_1 = 0.080$ and $\sigma_1/\sigma_y = 1.14$, it is clear that void coalescence is approaching, by necking of the ligament between the neighbouring different size voids. It is noted that due to the assumed symmetries plastic flow localization is predicted at the voids at either end of the unit cell. In the absence of such symmetry assumptions the simultaneous localization in many parallel layers would be unstable, and plastic flow localization would occur in only one layer.

The results in Fig. 4 for smaller initial void volume fractions show very similar behaviour, except that the onset of localization is more delayed the smaller the voids. Thus, for $f_1^* = 0.004$ plastic flow localization starts at $\varepsilon_1 = 0.28$ and for $f_1^* = 0.0004$ localization starts at $\varepsilon_1 = 0.51$. For both these cases Fig. 4c clearly shows that initially v_2/v_1 grows smaller than unity, so that the larger void grows relatively most rapidly. This is in very good agreement with the behaviour found earlier (Fig. 9 in Tvergaard, 1996) for the same range of void volume fractions. However, as soon as plastic flow localization occurs, the trend is opposite, $\dot{v}_2 > \dot{v}_1$, so that subsequently the ratio v_2/v_1 grows towards a value larger than unity, as was also found for $f_1^* = 0.04$.

In the following computations the focus is on much larger void size differences, in order to investigate the behaviour of a very small void in the stress fields near a larger void. This relates to the study of Faleskog and Shih (1997) for cylindrical voids; but more realistic spherical void shapes are considered in the present computations, and there are significant differences between the stress perturbations induced by spherical or cylindrical voids, respectively. In Fig. 5, for $A_0/R_0 = 10$ as in Figs 3 and 4 and for the same material parameters, the initial void volume fractions are specified by $(f_1^*)_I = 7 \times 10^{-4}$ and $(f_2^*)_I = 10^{-10}$, i.e. $R_1/R_0 = 0.219$ and $R_2/R_0 = 0.00114$. Also here, with large void size differences, the meshes at the two voids have been made closely identical, relative to void size.

The curves in Fig. 5 show comparisons for four different levels of stress triaxiality, corresponding to ρ values of 0.3, 0.5, 0.6, 0.7 and 0.9. For $\rho = 0.5$ localization of plastic flow in the layers containing the voids occurs of $\varepsilon_1 = 0.336$, for $\rho = 0.6$ localization occurs at $\varepsilon_1 = 0.147$, for $\varepsilon = 0.7$ and $\rho = 0.9$ localization occurs at $\varepsilon_1 = 0.0422$ and $\varepsilon_1 = 0.0079$, respectively. On the other hand, for $\rho = 0.3$ the computation has been continued until

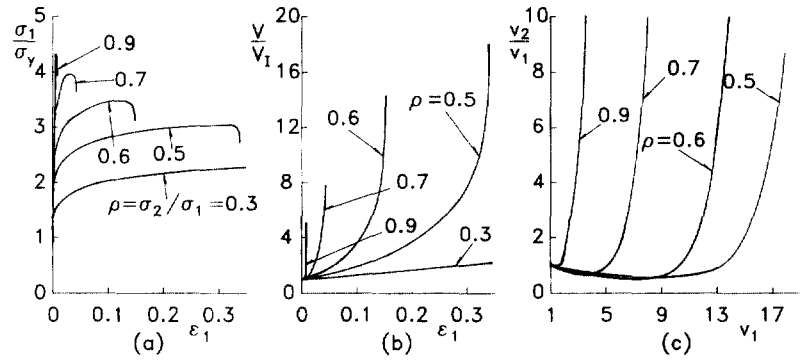

Fig. 5. Stress–strain curves and void growth for $A_0/R_0 = 10$, $(f_1^*)_I = 7 \times 10^{-4}$, $(f_2^*)_I = 7 \times 10^{-10}$. (a) Axial tensile stress vs strain. (b) Total void volume vs strain. (c) Growth of normalized void volumes.

$\varepsilon_1 = 1.08$ without reaching $(\sigma_1)_{max}$ or the onset of localization, and in this range v_2/v_1 has remained very close to unity.

Fig. 5b shows the relative increase of the total void volume, but the values shown for V/V_I are in fact practically identical to the values of v_1, since the void volume here is completely dominated by the volume of the larger void. Fig. 5c shows that the values v_2/v_1 initially tend to decay well below unity, as was also found in Fig. 4c for the two smaller void volume fractions. The growth of the ratio v_2/v_1 towards large values initiates when elastic unloading occurs outside the layers containing the voids. Thus, for the spherical voids considered here a strongly accelerated growth of very small voids due to the stress fields around neighbouring larger voids is not found, in contrast to the results of Faleskog and Shih (1997) for cylindrical voids. In the computations illustrated in Fig. 5 the very rapid growth of the small void (to values as large as $v_2/v_1 = 67$ for $\rho = 0.9$) is only a result of the plastic flow localization with elastic unloading outside the narrow layer containing the voids.

For $\rho = 0.9$ the stress triaxiality in the material is high enough so that a cavitation instability would occur for a single void in an infinite solid (Huang *et al.*, 1991; Tvergaard *et al.*, 1992). However, in Fig. 5, due to the rather large voids, the peak stress reached for $\rho = 0.9$ is only $\sigma_1/\sigma_y = 4.28$, well below the level 5.70 required for a cavitation instability. Also in the final growth stage in the localized band the local stress levels around the small void are not high enough to give unstable cavity growth; instead the macroscopic strain ε_1 keeps increasing slightly during void growth, and the larger void keeps growing slowly while the small void grows rapidly.

The definition of a cavitation instability may be unclear in cases with a finite void volume fraction, f. For a single void in an infinite solid the cavitation instability is reached when the void grows without bounds for a constant state of stress and strain at infinity. Void growth without further stress increase, $dV/d\sigma_1 \to \infty$, where V is the volume of one of the voids, is commonly reached in materials with a finite void volume fraction (e.g. see Tvergaard, 1982a), but this represents only the onset of damage induced softening. The condition $dV/d\varepsilon_1 \to \infty$ represents a real mechanical instability under prescribed edge displacements, and this is the condition used here to define a cavitation instability. By the same condition Tvergaard (1996, 1997) has determined cavitation instabilities in materials with a finite void volume fraction. It is noted that the occurrence of this cavitation instability condition is easily determined here, due to the special numerical procedure employed (see below eqn (2.11)).

The initial undeformed mesh for all the computations in Fig. 5 is shown in Fig. 6a. Furthermore, for the case where $\rho = 0.7$ a deformed mesh is shown in Fig. 6b corresponding to a stage where $\varepsilon_1 = 0.042$, $\sigma_1/\sigma_y = 3.50$, $v_1 = 9.26$ and $v_2 = 268.5$, i.e. well beyond the onset of plastic flow localization. The growth of the larger void is directly visible in Fig.

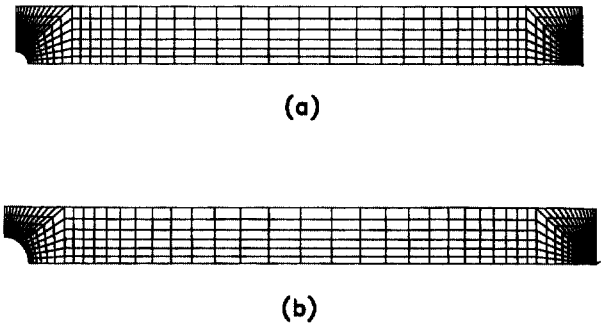

Fig. 6. Initial and deformed mesh for $A_0/R_0 = 10$, $\rho = 0.7$, $(f_1^*)_I = 7 \times 10^{-4}$, $(f_2^*)_I = 10^{-10}$. (a) At $\varepsilon_1 = 0$, $\sigma_1/\sigma_y = 0$. (b) At $\varepsilon_1 = 0.042$, $\sigma_1/\sigma_y = 3.50$, $v_1 = 9.26$, $v_2 = 269$.

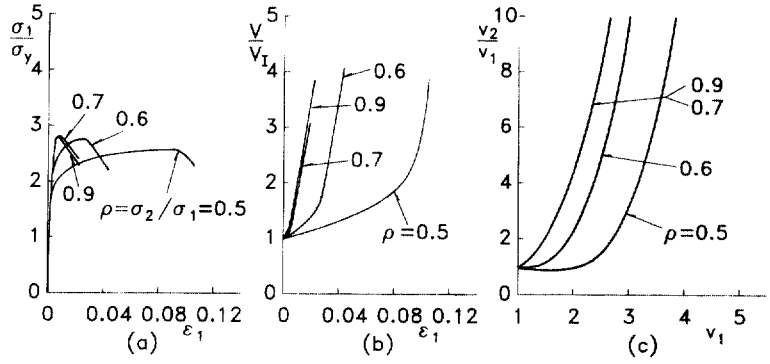

Fig. 7. Stress–strain curves and void growth for $A_0/R_0 = 10$, $(f_1^*)_I = 7 \times 10^{-3}$, $(f_2^*)_I = 10^{-10}$. (a) Axial tensile stress vs strain. (b) Total void volume vs strain. (c) Growth of normalized void volumes.

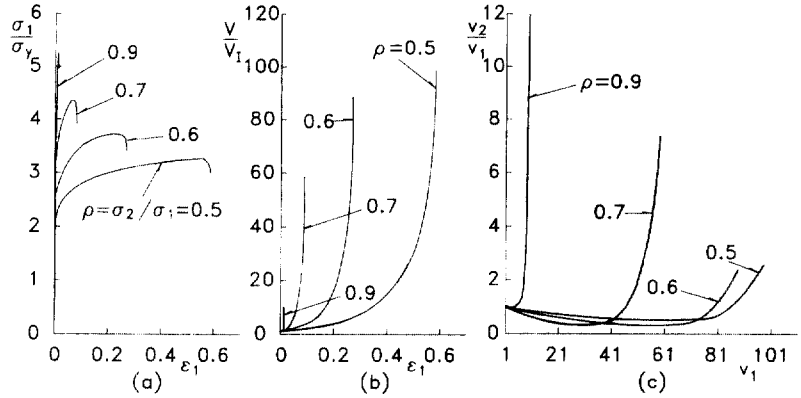

Fig. 8. Stress–strain curves and void growth for $A_0/R_0 = 10$, $(f_1^*)_I = 7 \times 10^{-5}$, $(f_2^*)_I = 10^{-10}$. (a) Axial tensile stress vs strain. (b) Total void volume vs strain. (c) Growth of normalized void volumes.

6b; but the smaller void is still so small that it cannot be seen in the figure, even though its relative growth has been much larger.

The effect of the initial size of the larger void is studied in Figs 7 and 8, in terms of results for a 10 times larger void, $(f_1^*)_I = 7 \times 10^{-3}$, or a 10 times smaller void, $(f_1^*)_I = 7 \times 10^{-5}$. In all these computations the initial size of the smaller void is kept unchanged, as specified by $(f_2^*)_I = 10^{-10}$. In Fig. 7, for the rather large void, there is a clear onset of localization for $\rho = 0.5$, but for the three larger values of ρ it appears that full plastic yielding never takes place in the central part of the unit cell between the two

voids. In all cases, the maximum stress levels reached are well below those reached in the corresponding cases in Fig. 5, and also, the strain ε_1 keeps increasing significantly after the maximum stress point, so that neither of these cases are anywhere near the occurrence of a cavitation instability at the small void. Thus, as in Fig. 5, the final more rapid growth of the smaller void illustrated in Fig. 7c is not basically a result of stress concentrations around the larger void, but occurs due to the localized plastic yielding and the associated more constrained plastic flow in the layers containing the voids.

In Fig. 8 the maximum stress levels reached are higher than those reached in Fig. 5, and much higher than those in Fig. 7. Also the values of the overall strain ε_1 at the onset of localization are much increased when the initial void size is reduced, as is seen by comparison of Figs 8, 5 and 7, and the same tendency is seen for the values of relative void growth, V/V_f and v_1. For the highest level of stress triaxiality, $\rho = 0.9$ in Fig. 8, the maximum average stress reached is $\sigma_1/\sigma_y = 5.20$, still well below the cavitation instability level of 5.70. Here, there is never complete plastic yielding in the central part of the unit cell, but the final mode of deformation is still dominated by localized plastic flow in the layers of material containing the voids. After that the peak stress is reached, the overall strain ε_1 grows very little, and also the value of v_1 grows only slowly, while the small void (v_2) grows rapidly. At this stage the local stress field around the small void is characterized by levels of hydrostatic tension, $\sigma_k^k/3$, around $5.1\sigma_y$, which is rather close to the level $\sigma_k^k/3 = 5.32\sigma_y$, at which a cavitation instability would occur for a single void in an infinite solid (Tvergaard *et al.*, 1992).

When the present unit cell analyses are employed to study material behaviour and fracture by void coalescence in front of a crack tip, the maximum average tensile stress is limited by the maximum stress levels reached ahead of the crack front. For a blunting crack tip in a power hardening elastic-plastic material with $N = 0.1$, $\sigma_y/E = 1/300$ and $\nu = 0.3$ McMeeking (1977) has computed the value of the maximum stress normal to the crack plane ahead of the cracks as $(\sigma_1/\sigma_y)_{\max} = 3.8$. For plastic yielding in material well ahead of the crack tip it is often assumed that a uniaxial strain state gives a good approximation, as can be represented in the present cell model by an appropriate choice of ρ (near unity) in each increment. However, the stress peak ahead of the crack, $(\sigma_1/\sigma_y)_{\max} = 3.8$, cannot be exceeded; in fact the peak stress reached is a good measure of the constraint on plastic flow enforced by the strain fields in the near tip region. Therefore, in terms of the present cell model analysis, the attainment of the correct value of the peak stress must be used to choose the value of ρ that gives the best approximation to the behaviour in front of a crack tip. Based on this criterion the appropriate values of ρ in Figs 5 and 8 are $\rho \simeq 0.67$ and $\rho \simeq 0.61$, respectively. But in Fig. 7 it is seen that the larger void is so dominant that the peak values reached for σ_1/σ_y are way below the value 3.8 for all levels of stress triaxiality considered. For the smaller values of $(f_1^*)_I$, in Figs 5 and 8, the curves showing a peak stress close to that ahead of a crack tip do not actually predict a cavitation instability for the tiny void between larger voids. The behaviour in these cases is strongly dominated by the occurrence of plastic flow localization, and the much faster growth of the small void is only predicted after the onset of localization, where the local constraint on plastic flow is suddenly changed due to elastic unloading outside the band.

The studies discussed so far have focused on cell models with $A_0/R_0 = 10$, thus representing interaction of different size voids inside isolated layers of material normal to the maximum tensile stress. By contrast, the studies in Tvergaard (1996) are carried out for about equal spacings in axial and transverse directions, $A_0/R_0 = 2$, which allows for interactions between neighbouring voids in the axial direction as well as the transverse directions. To get a parametric understanding of the effect of the spacing A_0 in the axial direction, computations have been carried out for values of A_0/R_0 ranging from 2 to 16, as illustrated in Fig. 9. These computations are carried out for $(f_1^*)_I = 7 \times 10^{-4}$, $(f_2^*)_I = 10^{-10}$ and $\rho = 0.7$, so that the curves for $A_0/R_0 = 10$ are identical to the curves for $\rho = 0.7$ in Fig. 5. Thus, in all cases the void radii relative to the cell radius are $R_1/R_0 = 0.219$ and $R_2/R_0 = 0.00114$, respectively. The computation for $A_0/R_0 = 2$ in Fig. 9 is not directly comparable with results in Tvergaard (1996), where the initial void volume ratios are 7, since in Fig. 9 the smaller void is extremely small compared to the larger void.

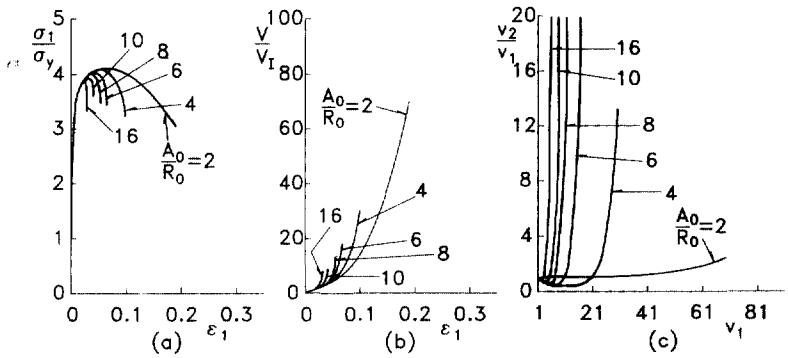

Fig. 9. Stress–strain curves and void growth for $A_0/R_0 = 10$, $\rho = 0.7$, $(f_1^*)_I = 7 \times 10^{-4}$, $(f_2^*)_I = 10^{-10}$. (a) Axial tensile stress vs strain. (b) Total void volume vs strain. (c) Growth of normalized void volumes.

In Fig. 9a it is seen that localization of plastic flow, with the resulting rapid decay of the average tensile stress, occurs earlier the larger the value of A_0/R_0, and the corresponding effect on the growth of the total void volume is seen in Fig. 9b. Also, in Fig. 9c, for A_0/R_0 in the range from 16 to 4, the ratio v_2/v_1 initially decays and then starts to grow rapidly when flow localization has occurred, as has been found in most of the previous figures. Only one of the cases, $A_0/R_0 = 2$, differs from the others in that no elastic unloading occurs in the unit cell between the two voids, and thus there is no flow localization. The effect of this difference is most clearly seen in Fig. 9c, where the ratio v_2/v_1 remains near unity during much void growth and then starts to increase rather slowly.

The comparison in Fig. 9 illustrates clearly that the very rapid growth of the tiny void between larger voids, as also found in the final stages of deformation in Figs 5, 7 and 9, is strongly dependent on the occurrence of elastic unloading in the material outside the layer containing the voids with the associated increase of the constraint on plastic flow. For the material with approximately equal void spacings in axial and transverse directions, $A_0/R_0 = 2$, where the relative spacings are approximately equal to those in the plane strain study of Faleskog and Shih (1997), the growth rate of the tiny void is not strongly amplified by the three dimensional stress fields around the larger spherical voids.

4. DISCUSSION

The present axisymmetric unit cell studies have been used to investigate the effect of cavitation instabilities on void coalescence in stress states corresponding to those in front of a growing crack. Even though the peak value of the average stress in front of a blunting crack is well below the stress level required for cavitation instabilities (Huang *et al.*, 1991; Tvergaard *et al.*, 1992), the local stress level in material between two larger voids is increased relative to the average stress, and very small voids in such regions could experience a cavitation instability. For a square array of larger cylindrical voids, in a plane strain unit cell study, Faleskog and Shih (1997) have found some indication that this type of void coalescence mechanism could be active. The axisymmetric analyses with the special boundary conditions used in the present paper allow for a relatively simple investigation of similar behaviour in a full three dimensional array of spherical voids, without having to solve the full three dimensional numerical problem.

A fixed ratio ρ of the average true stresses in transverse and axial directions is prescribed in the present cell model studies. This may not exactly reproduce stress states in front of crack tips, but it is fairly easy in each case to identify the maximum value of ρ that could be relevant, since the predicted stress maximum cannot exceed the peak stress ahead of a crack in a void free material. For the smallest void volume fraction analysed here, this means that the value of ρ cannot exceed 0.61, which is far below the value required for unstable growth of a single cavity in an infinite solid. Thus a cavitation instability for a small void would have to rely on local stress increases between the larger voids; but none

of the cases studied have shown such behaviour in the relevant range of ρ values. For a case with about equal void spacings in axial and transverse directions ($A_0/R_0 = 2$), somewhat similar to the spacings used by Faleskog and Shih (1997), the present predictions are nowhere near unstable growth of the smaller void. It must be concluded that the effects of local stress increases in material between larger voids is much less dominant in a three dimensional array of spherical voids than that found in a plane strain study for cylindrical voids.

Localization of plastic flow plays an important role in most of the present studies, where the axial void spacing has been chosen much larger than the transverse spacing (often $A_0/R_0 = 10$). Here, elastic unloading occurs throughout most of the unit cell shortly after the maximum load point, and all subsequent plastic flow is concentrated in the thin layers of material containing the voids. In such thin layers of elastic–plastic material between elastic material regions plastic flow is highly constrained, and it is well known that sufficiently small voids in such layers will experience cavitation instabilities (Tvergaard, 1991, 1997). In the present studies, where small voids interact with much larger voids inside the thin plastic layers, a full cavitation instability is not reached; but some cases are close, and all cases show much more rapid growth of the smaller voids after the onset of localization.

Simultaneous localization of plastic flow in a number of parallel material layers, as predicted by the present cell model, is a feature of the periodicity assumed in the cell model; but the interest here is only in the interaction between different size voids within one of the layers. In the highly strained region just ahead of a crack tip only one such material layer with void growth to coalescence tends to develop, due to the highly nonuniform strain field (see Needleman and Tvergaard, 1987; Tvergaard and Needleman, 1992). In cases where deformations occur at a high rate, e.g. inside an adiabatic shear band as studied by Cortés and Elices (1993), thermal softening will occur, and this may further promote the possibility of unstable cavity growth.

An actual alloy may contain more than two size scales of inclusions. For such alloys it has been suggested by Faleskog and Shih (1997) that a process of cavitation instability at very small voids, induced by local stress increases between larger neighbouring voids, will repeat itself with the even smaller size scale of voids, thus giving rise to cascading load drops. This kind of effect might enhance the influence of different size scales, even in the full three dimensional array of voids. But there is an opposite effect of size, discussed by Fleck and Hutchinson (1996) in the context of strain gradient plasticity, which has not been included in the present analyses for spherical voids, nor in the previous plane strain study for cylindrical voids. It is suggested based on dislocation theory that the plastic flow strength increases significantly if the plastic strain gradient is large over distances comparable with the dislocation spacing or the elastic cell size within the dislocation structure, and this would strongly reduce predicted growth rates for very small voids.

REFERENCES

Ashby, M. F., Blunt, F. J. and Bannister, M. (1989) Flow characteristics of highly constrained metal wires. *Acta Metallurgica* **37,** 1857.

Ball, J. M. (1982) Discontinuous equilibrium solutions and cavitation in nonlinear elasticity. *Phil. Trans. R. Soc. London* **A306,** 557–610.

Cortés, R. and Elices, M. (1993) The plastic growth of a cavity nucleated at a shear band. *Int. J. Solid Structures* **21,** 2971–2981.

Faleskog, J. and Shih, C. F. (1997) Micromechanics of coalescence—I. Synergistic effects of elasticity, plastic yielding and multi-size scale voids. *J. Mech. Phys. Solids* **45,** 21–50.

Fleck, N. A. and Hutchinson, J. W. (1996) Strain gradient plasticity. to be published in *Advances in Applied Mechanics*, ed. J. W. Hutchinson and T. Y. Wu, **33,** Academic Press, New York.

Huang, Y., Hutchinson, J. W. and Tvergaard, V. (1991) Cavitation instabilities in elastic–plastic solids. *J. Mech. Phys. Solids* **39,** 223–241.

Hutchinson, J. W. (1973) Finite strain analysis of elastic–plastic solids and structures. In *Numerical Solution of Nonlinear Structural Problems*, ed. R. F. Hartung, p. 17. ASME, New York.

Koplik, J. and Needleman, A. (1988) Void growth and coalescence in porous plastic solids. *Int. J. Solids Structures* **24,** 835–853.

McClintock, F. A. (1968) A criterion for ductile fracture by growth of holes. *J. Appl. Mech.* **35,** 363–371.

McMeeking, R. M. (1977) Finite deformation analysis of crack-tip opening in elastic–plastic materials and implications for fracture. *J. Mech. Phys. Solids* **25,** 357–381.

Needleman, A. (1972) Void growth in an elastic–plastic medium. *J. Appl. Mech.* **41,** 964–970.

Needleman, A. and Tvergaard, V. (1987) An analysis of ductile rupture modes at a crack tip. *J. Mech. Phys. Solids* **35,** 151–183.

Rice, J. R. and Tracey, D. M. (1969) On the ductile enlargement of voids in triaxial stress fields. *J. Mech. Phys. Solids* **17,** 201–217.

Tvergaard, V. (1976) Effect of thickness inhomogeneities in internally pressurized elastic–plastic spherical shells. *J. Mech. Phys. Solids* **24,** 291–304.

Tvergaard, V. (1981) Influence of voids on shear band instabilities under plane strain conditions. *Int. J. Fracture* **17,** 389–407.

Tvergaard, V. (1982a) On localization in ductile materials containing spherical voids. *Int. J. Fracture* **18,** 237–252.

Tvergaard, V. (1990) Analysis of tensile properties for a whisker–reinforced metal–matrix composite. *Acta Metall. Mater.* **38,** 185–194.

Tvergaard, V. (1991) Failure by ductile cavity growth at a metal–ceramic interface. *Acta Metall. Mater.* **39,** 419–426.

Tvergaard, V. (1996) Effect of void size difference on growth and cavitation instabilities. *J. Mech. Phys. Solids* **44,** 1237–1253.

Tvergaard, V. (1997) Studies of void growth in a thin ductile layer between ceramics. *Computational Mech.* **20,** 186–191.

Tvergaard, V. and Needleman, A. (1992) Effect of crack meandering on dynamic, ductile fracture. *J. Mech. Phys. Solids* **40,** 447–471.

Tvergaard, V., Huang, Y. and Hutchinson, J. W. (1992) Cavitation instabilities in a power hardening elastic–plastic solid. *Eur. J. Mech. A/Solids* **11,** 215–231.